A Novel Sensorless MPPT Controller for a High-Efficiency Microscale Wind Power Generation System

Ching-Tsai Pan, *Member, IEEE*, and Yu-Ling Juan, *Student Member, IEEE*

***Abstract*—In this paper, a novel maximum power point tracking (MPPT) controller with an adaptive compensation control is first proposed for a microscale wind power generation system (WPGS). Based on the adaptive control, the dynamic response is improved and more wind energy can be captured during wind velocity variations. For cost and reliability consideration, no mechanical sensors are used in this proposed WPGS. A single-stage ac-to-dc converter is then proposed to replace the traditional two-stage converter and incorporate the MPPT control for achieving higher efficiency and lower total harmonic distortion (THD). To further improve the efficiency of the converter, a quasi-synchronous rectification (QSR) algorithm is proposed to control the active switches for reducing the conduction loss of the body diodes. The analytic closed form duty ratios of the corresponding active switches are also derived for easy implementation. Furthermore, a prototype system is constructed and the proposed MPPT controller and QSR algorithm are both implemented using a DSP, namely, TMS320F2812. Some experimental results are given to verify the validity of the proposed microscale WPGS. It is found that the total output energy can be increased by 13% for the microscale WPGS.**

***Index Terms*—High efficiency, maximum power point tracking (MPPT), wind power generation system (WPGS).**

I. Introduction

RECENTLY, various renewable energy resources have attracted a lot of attention because they are pollution-free and inexhaustible. The wind power generation system (WPGS) is one of the most effective power generation systems that convert the wind energy into some specific forms of electricity. From the viewpoint of cost–performance ratio, most of the WPGSs are large-scale ones. However, the small-scale WPGSs can also provide another alternative that, in fact, is more suitable for the urban environment than the large-scale ones due to the limited space and safety consideration. According to a recent small wind turbine global market study made by the American Wind Energy Association in 2007 [1], approximately 6800 Americans purchased small WPGSs and the corresponding installed capacity in U.S. is about 17.5 MW. The microscale WPGS is a subset of the small-scale ones and by definition its capacity is less than 1 kW.

Typically, a microscale WPGS is composed of a wind turbine with a fixed pitch angle, a permanent-magnet (PM) generator, a diode bridge rectifier, a dc converter, a battery power module, and a dc load. In order to make the WPGS more efficient, a maximum power point tracking (MPPT) control strategy is necessary for maximizing the output power. Basically, the MPPT technique can roughly be classified into the following four strategies, namely, the tip speed ratio (TSR) control, the optimal torque (OT) control [2], [3], the power mapping control [4], [5], and the perturbation and observation (P&O) searching control [6], [7].

For the TSR control, an expensive anemometer is required to achieve maximum output control. As to the OT control strategy, the well-known OT, namely, $k\omega_m^2$, is adopted as the command signal for controlling the generator torque to maximize the output power. Similarly, for the power mapping control, the well-known optimal output power command, namely, $k\omega_m^3$, is adopted for controlling the generator output power. Practically, the wind velocity is changing all the time. The steady-state wind velocity is in fact very unusual. Hence, as the wind speed is either increased or decreased, if the rotor speed of the generator cannot track the variation of the wind speed closely, then the extracted wind energy will be reduced greatly. In fact, to the authors' best knowledge, most existing papers consider only the tracking along the maximum power trajectory of $k\omega_m^3$ or the OT trajectory of $k\omega_m^2$. Very few papers concern about the effect of the WPGS inertia on the wind energy capturing. As to the P&O control, although it has the advantages of simplicity and flexibility, the oscillating control around the optimal point will certainly sacrifice the efficiency of the WPGS. However, for a microscale WPGS, the power coefficient function of the turbine can be measured easily, which enables one to obtain the *k*-coefficient of the OT. Hence, the mechanic sensorless OT control can be implemented easily to reduce cost.

On the other hand, due to cost reduction consideration, a full diode bridge rectifier is always adopted to convert the three-phase ac voltage of the generator into dc voltage. Then, a dc converter is needed as the second stage to achieve MPPT control. It is well known that the efficiency of a two-stage converter is always poorer than a single stage due to the twice power conversions. Moreover, the diode voltage drops and the significant current total harmonic distortion (THD) will also reduce the efficiency of the WPGS significantly. In view of the above drawbacks, it is the major motivation of this paper to propose a novel MPPT controller and a quasi-synchronous rectification (QSR) single-stage ac-to-dc converter for a microscale WPGS such that more wind energy can be extracted while the wind speed is under variation and less electrical energy is dissipated in the ac-to-dc converter with little additional cost. It turns out

Manuscript received January 13, 2009; revised April 27, 2009. First published November 24, 2009; current version published February 17, 2010. This work was supported in part by the National Science Council of R.O.C. under Grant NSC 96-2218-E-007-003 and Grant NSC 96-2221-E-007-171-MY3. Paper no. TEC-00490-2008.

The authors are with the Department of Electrical Engineering, National Tsing Hua University, Hsinchu 300, Taiwan (e-mail: ctpan@ee.nthu.edu.tw; d927901@oz.nthu.edu.tw).

Digital Object Identifier 10.1109/TEC.2009.2032604

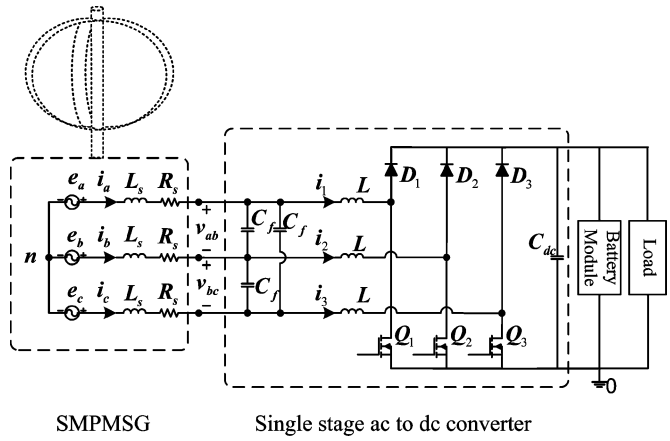

Fig. 1. Configuration of the proposed WPGS.

that with the proposed WPGS, the total generated energy can be increased greatly.

The remaining contents of this paper are organized as follows. First, the proposed system configuration is described in Section II. Second, the proposed sensorless MPPT controller is then presented in Section III. In Section IV, the proposed QSR ac-to-dc converter is depicted in detail. Some experimental results are then given in Section V to verify the validity of the proposed system. Finally, some conclusions are given in the last section.

II. System Configuration of the Proposed WPGS

The configuration of the proposed microscale WPGS is shown in Fig. 1. From Fig. 1, one can see that the system, basically, consists of a typical fixed pitch angle wind turbine, a surface-mounted permanent synchronous generator (SMPMSG), a semicontrolled ac-to-dc converter, a battery module, and a dc load. The load may be an inverter for supplying standalone ac electricity or connecting to the utility directly.

The output power P_w of the wind turbine can be expressed as follows [2]:

$$P_w = \frac{1}{2}\rho C_p A v_w^3 \tag{1}$$

where

- ρ the air density;
- A the effective area swept by the wind turbine;
- v_w the wind speed;
- C_p the power coefficient of the wind turbine.

The power coefficient is a function of the TSR δ defined as follows:

$$\delta = \frac{r\omega_m}{v_w} \tag{2}$$

where r is the radius of turbine blade and ω_m is the rotor speed. The measured power coefficient of the microscale wind turbine used in this paper is shown in Fig. 2 for reference. From the measured C_P shown in Fig. 2, one can find an approximate polynomial to represent the C_P function as follows:

$$C_p(\delta) = a_0 + a_1\delta + a_2\delta^2 + a_3\delta^3 + a_4\delta^4 \tag{3}$$

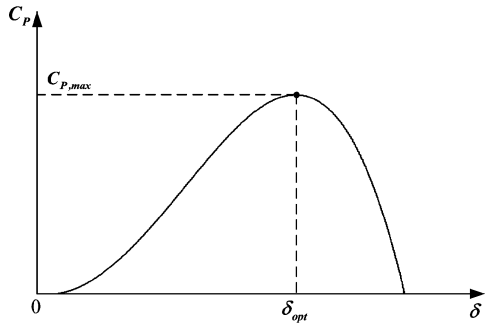

Fig. 2. Power coefficient function of the wind turbine adopted in this paper.

where $a_0 - a_4$ are real constants. It is found from the previous analytic expression that the corresponding maximum power coefficient, namely, $C_{p,\max}$, and optimal TSR, $\delta_{\rm opt}$, can be obtained directly. It follows from (1) and (2) that the maximum output power and optimal output torque of the wind turbine can be expressed as follows:

$$P_{w,\max} = k\omega_m^3 \tag{4}$$

$$T_{w,\rm opt} = k\omega_m^2 \tag{5}$$

where $k = (0.5\rho A r^3 C_{p,\max})/\delta_{\rm opt}^3$. Due to its high efficiency and high power density, an SMPMSG is usually adopted to convert the wind energy into electric energy. The corresponding dynamic model in the stationary reference frame with space vector notation [8] is given as follows:

$$\vec{v}_s^{\,s} = -R_s\vec{i}_s^{\,s} + \frac{d}{dt}\vec{\lambda}_s^{\,s} \tag{6}$$

$$\vec{\lambda}_s^{\,s} = -L_s\vec{i}_s^{\,s} + \vec{\lambda}_r^{\,s} \tag{7}$$

$$\vec{\lambda}_r^{\,s} = \lambda_f e^{j\theta} \tag{8}$$

where λ_f is the magnitude of the flux linkage due to the permanent magnet, θ is the angle between the magnetic axis of the stator a-phase winding and the direct axis of the rotor, R_s and L_s are the winding resistance and the stator inductance, respectively. For convenient analysis of the ac-to-dc converter, one can define the back EMF $\vec{e}_s^{\,s}$ of the SMPMSG as follows:

$$\vec{e}_s^{\,s} \equiv \frac{d}{dt}\vec{\lambda}_r^{\,s} = j\frac{d\theta}{dt}\lambda_f e^{j\theta}. \tag{9}$$

From (6) to (9), one can get the corresponding stator phase voltage equations as follows:

$$v_{jn} = -R_s i_j - L_s\frac{di_j}{dt} + e_j, \qquad j \in \{a,b,c\} \tag{10}$$

where

$$E \equiv \lambda_f\frac{d\theta_e}{dt}, \qquad \theta_e \equiv \theta + \frac{\pi}{2}. \tag{11}$$

From (10) and (11), one can get the equivalent circuit of the generator, as shown in Fig. 1. Also, the dynamic model of the corresponding mechanical system can be represented as follows:

$$T_w - T_g = J\frac{d\omega_m}{dt} + B\omega_m \tag{12}$$

$$T_g \equiv k_t I_m = \frac{3}{2}\frac{P}{2}\lambda_f I_m \tag{13}$$

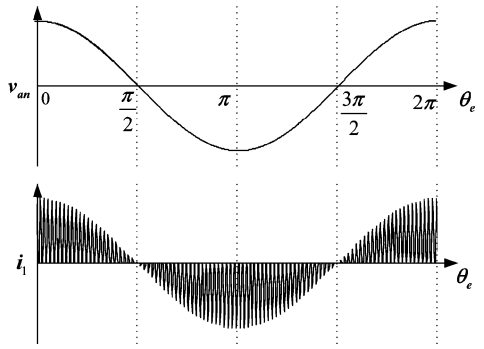

Fig. 3. Inductor current and the phase voltage waveforms of phase a.

where T_w and T_g are the wind power torque and generator torque, respectively, J is the total inertia of the WPGS, B is the viscous damping coefficient, P is the number of poles, and I_m is the amplitude of the phase current.

Next consider the adopted semicontrolled ac-to-dc converter, as shown in Fig. 1. From Fig. 1, one can see that a delta connected capacitor filter is connected at the generator terminals to filter out the high frequency switching ripple of the ac-to-dc converter. As a compromise of both efficiency and cost considerations, three low-ON-resistance MOSFETs are used to replace half of the diodes of the traditional full diode bridge. In other words, this single-stage converter is chosen to replace the traditional two-stage converter consisting of a full diode bridge rectifier and a dc-to-dc converter for MPPT. It is well known in power electronics that if the inductor currents are controlled in discontinuous conduction mode (DCM), then the resulting peak currents will automatically follow the sinusoidal phase voltages, as shown in Fig. 3. In other words, after filtering out the high frequency components, the generator currents will be sinusoidal and the I^2R loss in the generator windings will be reduced. Furthermore, the sixth-order harmonics appear at the dc output terminal can be avoided that not only renders the MPPT control much easier but also can achieve better efficiency.

III. Novel Sensorless MPPT Control With an Adaptive Control

As mentioned before, although the optimal torque or power can be calculated easily, however, due to the inertia of the mechanical system, it is not possible to achieve instantaneous tracking as the wind velocity is changing rapidly. This situation becomes even worse when the wind speed is in the low speed region where the acceleration or deceleration torque is rather small if an existing MPPT controller is adopted. As a result, the extracted energy in fact is significantly less than the maximum energy available. To overcome this dilemma, a novel MPPT controller is proposed in this section. Fig. 4 shows the block diagram of the proposed MPPT controller. From Fig. 4, one can see that the proposed MPPT controller is composed of four blocks where block A is the rotor speed estimator (RSE), block B is the wind power torque estimator (WPTE), block C is the proposed novel torque command calculator (NTCC) for MPPT, and block D is the generator current controller (GCC). First, consider the rotor

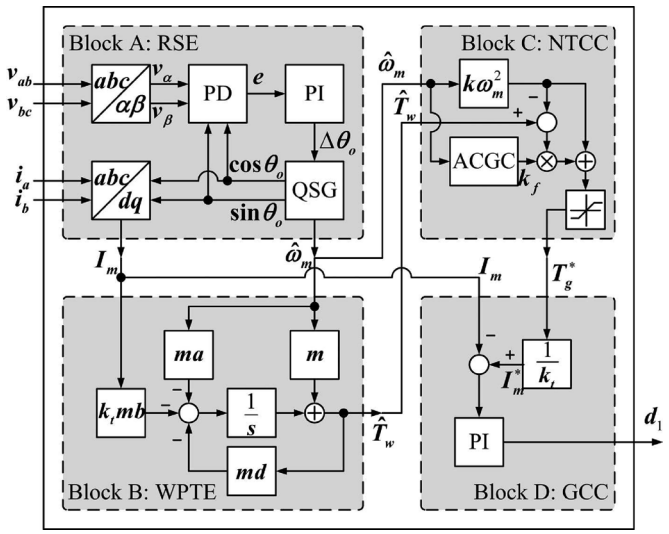

Fig. 4. Block diagram of the proposed MPPT controller.

speed estimator, as shown in block A. For microscale WPGS, the voltage drops of the stator inductances and the winding resistances are small enough and can be neglected. Therefore, the terminal voltages can be considered to be equal to the back EMFs approximately and the two phase input signals, v_α and v_β in block A, can be derived from the line voltages as follows:

$$\begin{bmatrix} v_\alpha \\ v_\beta \end{bmatrix} = \begin{bmatrix} 1 & 0 \\ \frac{1}{\sqrt{3}} & \frac{2}{\sqrt{3}} \end{bmatrix} \begin{bmatrix} v_{ab} \\ v_{bc} \end{bmatrix} \cong \begin{bmatrix} \sqrt{3}E\cos\left(\theta_e + \frac{\pi}{6}\right) \\ \sqrt{3}E\sin\left(\theta_e + \frac{\pi}{6}\right) \end{bmatrix}. \tag{14}$$

Consider the time-varying rotating speed, a two-phase type phase-locked-loop (PLL) algorithm [9], which is independent of the speed, is adopted for estimating the rotor speed. It is seen from block A that the phase difference e can be obtained through a two-phase detector (PD) and a quadrature signal generator (QSG). Mathematically, the output of the two-phase PD can be expressed by the following equation:

$$\begin{aligned} e &= v_\beta \cos\theta_o - v_\alpha \sin\theta_o \\ &= \sqrt{3}E\sin\left[\left(\theta_e + \frac{\pi}{6}\right) - \theta_o\right]. \end{aligned} \tag{15}$$

where θ_o is the phase angle of the generated quadrature unit signals. When the phase angle of the generated signals is close to that of the input signals of the PD, i.e., $\theta_o \cong \theta_e + \pi/6$, the corresponding phase difference can be approximated as follows:

$$e \cong \sqrt{3}E\left[\left(\theta_e + \frac{\pi}{6}\right) - \theta_o\right]. \tag{16}$$

After the refinement through a proportional–integral (PI) controller, the refined phase difference, namely, $\Delta\theta_o$, is obtained from the PI controller, as shown in block A. In this paper, the proposed controller is implemented by using a DSP (TMS320 F2812) and the phase angle of the generated signals is based on the following difference equation.

$$\theta_o(k) = \theta_o(k-1) + \Delta\theta_o(k). \tag{17}$$

If the input signals are not in phase with the generated signals of QSG, i.e., $e \neq 0$, then the output signal of the PI controller will be varied for adjusting the phase angle and the frequency of the generated signals from the QSG. Hence, as the PLL is locked, $\Delta\theta_o$ will remain constant and the corresponding electric frequency and the rotor speed can be obtained as follows:

$$\hat{\omega}_e = \frac{P}{2}\hat{\omega}_m = \frac{\Delta\theta_o}{T_s} \tag{18}$$

where T_s is the sampling time. As a byproduct, the amplitude of the generator current can also be obtained according to the following equation:

$$I_m = \vec{i}_s^{\,s} \cdot e^{-j\theta_e} = (i_\alpha + j i_\beta) \cdot e^{-j(\theta_o - \pi/6)} \tag{19}$$

where $i_\alpha = i_a$ and $i_\beta = (i_a + 2i_b)/\sqrt{3}$.

Second, consider the wind power torque estimator, as shown in block B, where a reduced order estimator [10] is adopted to determine the wind power torque. Because the sampling time is much smaller than the mechanical time constant, the wind power torque can be considered as a constant within a sampling period. According to the reduced-order estimator described in [10], the wind torque estimator can be expressed as

$$\dot{\hat{T}}_w = m(\dot{y} - ay - bT_g - d\hat{T}_w) \tag{20}$$

where $a = -B/J$, $b = -d = -1/J$, and m is the loop gain of the estimator. Then, the resulting dynamic equation of the estimation error can be derived as

$$\begin{aligned}\dot{\tilde{T}}_w &= \dot{T}_w - \dot{\hat{T}}_w \\ &= -m(\dot{\omega}_m - a\omega_m - bT_g - d\hat{T}_w) \\ &= -md(T_w - \hat{T}_w) = -md\tilde{T}_w\end{aligned} \tag{21}$$

where $\tilde{T}_w$ is defined as the estimation error of the wind power torque. Consequently, one can choose a proper time constant, namely, md, for fast converging of the estimation error.

Third, to track the maximum power point, block C is used to determine the torque command for the generator from the estimated rotor speed and the wind power torque. In order to overcome the mechanic inertia effect, an adaptive control effort with a proportional gain, k_f, is introduced to compensate for the torque command, as shown in block C during the transient period of the rapidly changing wind speed. The resulting torque command of the proposed controller will then assume the following form:

$$T_g^* = (\hat{T}_w - k\hat{\omega}_m^2) \cdot k_f + k\hat{\omega}_m^2. \tag{22}$$

From (22), one can observe that, under steady state, the resulting torque command T_g^* is just equal to the familiar OT of $k\omega_m^2$. However, during transient period, an adaptive compensation control is added for achieving faster response such that more wind energy can be captured.

Finally, consider the GCC, as shown in block D that will force the amplitude of the generator phase current I_m to converge to the reference signal, $I_m^* = T_g^*/k_t$.

Because the dynamic response speeds of the two estimators and the GCC are much faster than that of the mechanical system, the following conditions can be assumed true after a short transient:

$$T_g \cong T_g^* \qquad \hat{T}_w \cong T_w \qquad \hat{\omega}_m \cong \omega_m. \tag{23}$$

Hence, from (12), (22), and (23), one can get the resulting mechanical dynamic equation of the proposed WPGS as follows:

$$T_w - k\omega_m^2 = J_V \frac{d\omega_m}{dt} + B_V \tag{24}$$

where $J_V = J/(1 - k_f)$ and $B_V = B/(1 - k_f)$. To understand the merit of the proposed MPPT controller, one can consider the dynamic response of the mechanical system at different wind speed. Assume that the small signal disturbances around the operating points can be expressed as follows:

$$\omega_m = \omega_{mo} + \Delta\omega_m \tag{25}$$

$$v_w = v_{wo} + \Delta v_w \tag{26}$$

where ω_{mo} and v_{wo} are the rotor speed and wind speed of the operating points, and $\Delta\omega_m$ and Δv_w are considered as the small disturbance signals around the operating points, respectively. By substituting (3), (25), and (26) into (24) and taking linearization, the transfer function of Δv_w to $\Delta\omega_m$ can be obtained as follows:

$$\frac{\Delta\omega_m(s)}{\Delta v_w(s)} = \frac{N}{s + M} \tag{27}$$

where

$$N \equiv (1 - k_f)k_N\omega_{mo} \tag{28}$$

$$M \equiv (1 - k_f)k_M\omega_{mo} + \frac{B}{J} \tag{29}$$

$$k_N \equiv \frac{\rho r^2 A}{2J\delta_{\text{opt}}^2}(3a_0 + 2a_1\delta_{\text{opt}} + a_2\delta_{\text{opt}}^2 - a_4\delta_{\text{opt}}^4) \tag{30}$$

$$k_M \equiv \frac{\rho r^3 A}{2J\delta_{\text{opt}}^3}(a_0 - a_2\delta_{\text{opt}}^2 - 2a_3\delta_{\text{opt}}^3 - 3a_4\delta_{\text{opt}}^4) + \frac{2k}{J}. \tag{31}$$

One can see from (27) and (29) that the 3 dB bandwidth, $\omega_B(=M)$, is a function of k_f and ω_{mo}. For a traditional OT control strategy, the bandwidth will become narrower in low wind speed range. The slow dynamic response due to the narrow bandwidth will result in reduction of extracted wind energy during wind speed variation period. For the proposed MPPT controller, the bandwidth can be adjusted according to the rotor speed for obtaining more uniform dynamic response. Consequently, if the bandwidth is designed to be kept constant for achieving more uniform dynamics, the adaptive compensation gain should change with the rotor speed as follows:

$$k_f = f(\omega_m) = 1 - \frac{\omega_B - B/J}{k_M\omega_m}. \tag{32}$$

In fact, the adaptive compensation gain calculator (ACGC), as shown in block C, is implemented according to (32).

As an illustration of the merit of the proposed MPPT controller, consider the specific situation of the step change of wind velocity from V_{w1} to V_{w2} or *vice versa*. Due to the inertia of the WPGS, the generator speed cannot follow immediately the

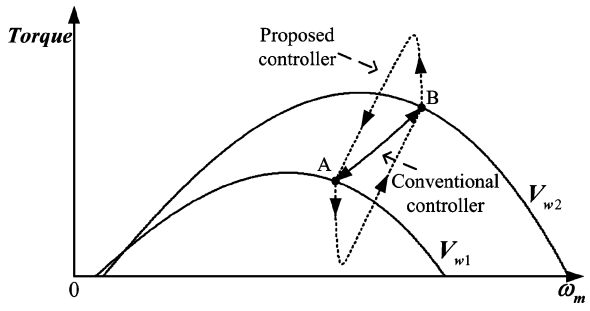

Fig. 5. Loci of the dynamic-state and the steady-state torque commands.

sudden speed change. For a conventional MPPT controller, the $k\omega_m^2$ command is adopted during the transient state, as shown in Fig. 5. However, as the wind velocity is suddenly changed to V_{w2}, the truly optimal command is located at point *B*. In other words, the solid trajectory between A and B is not the truly optimal trajectory. Hence, by using the conventional MPPT controller, the WPGS will be accelerated only by the torque difference between the input wind torque and the $k\omega_m^2$ command torque. In other words, the dynamic response of accelerating to the truly optimal operation point *B* will be rather slow. On the other hand, by using the proposed MPPT controller, due to the adaptive compensation, the torque command will be made smaller instantly than that of the conventional OT controller to increase the torque difference for faster accelerating to the truly optimal operation point *B*. Similarly, if the wind velocity is changed suddenly from V_{w2} to V_{w1}, contrast to the conventional OT controller, the torque command of the proposed MPPT controller will be made larger instantly for quickly decelerating the WPGS to the optimal point *A*. Consequently, the amount of the captured wind energy during the wind speed variation period can be increased significantly by using the proposed MPPT controller.

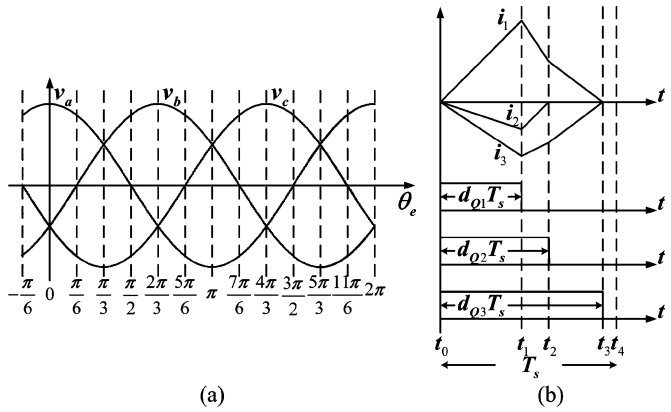

Fig. 6. Waveforms of (a) stator voltages of the generator. (b) Inductor currents and gating signals in one switching period.

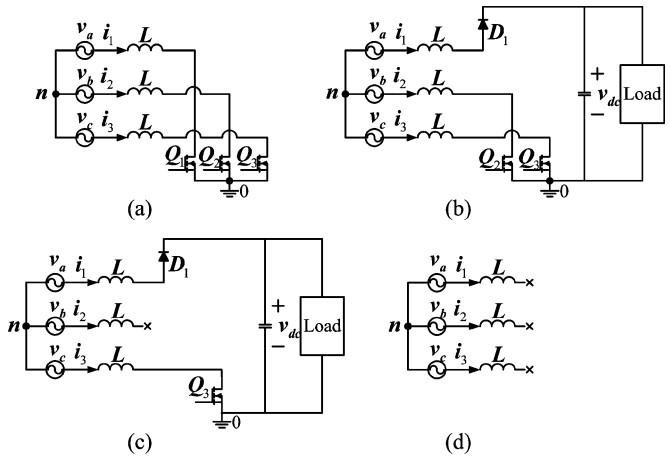

Fig. 7. The equivalent circuits of (a) mode I, (b) mode II, (c) mode III, and (c) mode IV.

IV. Quasi-Synchronous Rectification AC-to-DC Converter

Due to the nonlinearity of the diode bridge rectifier, the conventional microscale WPGS will induce a large amount of harmonic components in the generator output currents. Therefore, the generator output power will also contain remarkable ripple power components, which will be harmful to the mechanical shaft and generate low-frequency acoustic noise. The proposed semicontrolled rectifier is operated in DCM as mentioned in Section II to achieve nearly unit power factor and low-current THD. Moreover, the conduction losses of the diodes are significant in the low voltage application such as the microscale WPGS. Instead of using the single switch rectifier proposed in [11], a semicontrolled rectifier, as shown in Fig. 1 is adopted for reducing the conduction loss during the energy-increasing interval of the three boost inductors. Furthermore, a QSR technique is proposed for reducing the conduction loss caused by the body diodes during the energy-decreasing interval of the inductors. As a result, the efficiency of the front stage in the microscale WPGS will be greatly improved. For convenient illustration of the proposed QSR control method, the following assumptions are given first.

1) The switching frequency is much higher than the electrical frequency of the voltage sources.
2) The devices are considered as ideal components except the forward voltage drop of the diodes.
3) The terminal phase voltages can be approximated by three-phase back EMFs.

The three-phase voltages shown in Fig. 6(a) can be divided into twelve intervals. The proposed rectifier is analyzed in the interval $0 \le \theta_e \le \pi/6$ as an example to illustrate the proposed quasi-synchronous rectification technique for controlling the three active switches. The waveforms of the inductor currents and the gating signals in one switching period are shown in Fig. 6(b). There are four operation modes for the proposed rectifier in one switching period and the equivalent circuits of the operation modes shown in Fig. 7 are analyzed as follows.

1) Mode I ($t_0 \le t \le t_1$): In the first operation mode, all the active switches are turned on simultaneously for increasing the energy stored in the three inductors. The corresponding equivalent circuit is shown in Fig. 7(a). Hence, the inductor currents

can be expressed as follows:

$$\bar{i}(t) = \frac{t - t_0}{L} \cdot \bar{v}(t) \tag{33}$$

where $\bar{i}(t) = [\, i_1(t)\ i_2(t)\ i_3(t)]^T$, $\bar{v}(t) = [\, v_a(t)\ v_b(t)\ v_c(t)]^T$. The first operation mode is ended at $t = t_1$ and the peak value of the inductor currents is given by

$$\bar{i}(t_1) = \frac{d_1 T_s}{L} \cdot \bar{v}(t_1) \tag{34}$$

where $d_1 = (t_1 - t_0)/T_s$ is the duty ratio of the first operation mode and T_s denotes the switching period. According to (34), one can see that if the duty ratio d_1 is constant, the peak values of the three inductor currents will be proportional to the magnitude of the three-phase voltages respectively, as shown in Fig. 3. Therefore, after filtering out the high frequency components, the generator output currents will nearly be sinusoidal and in phase with the phase voltages.

2) Mode II ($t_1 \le t \le t_2$): During the second operation mode, the active switch Q_1 is turned off but the other switches Q_2 and Q_3 are still turned on, as shown in Fig. 7(b), to reduce the conduction loss caused by body diodes. The energy stored in the three inductors is decreased and the corresponding dynamic equations are given as follows:

$$L\frac{di_1}{dt} = v_a - V_{\rm df} - V_{\rm dc} - v_{\rm ON} \tag{35}$$

$$L\frac{di_2}{dt} = v_b - v_{\rm ON} \tag{36}$$

$$L\frac{di_3}{dt} = v_c - v_{\rm ON}. \tag{37}$$

The three-phase voltages are assumed to be balanced and the neutral point is floating. The voltage between the ground and the neutral point can be obtained as

$$v_{\rm ON} = -\frac{1}{3}(V_{\rm df} + V_{\rm dc}). \tag{38}$$

Hence, (35)–(37) can be rewritten as follows:

$$L\frac{d\bar{i}(t)}{dt} = \bar{v}(t) + H \cdot V_{\rm eq} \tag{39}$$

where $H = [-2/3 \quad 1/3 \quad 1/3]^T$, $V_{\rm df}$ is the forward voltage drop of the diode, and $V_{\rm eq} = V_{\rm df} + V_{\rm dc}$ is defined as the equivalent dc voltage. Consequently, the three inductor currents in the second mode are expressed as

$$\bar{i}(t) = \frac{t - t_1}{L}[\bar{v}(t) + H \cdot V_{\rm eq}] + \bar{i}(t_1). \tag{40}$$

The magnitude of the inductor current $i_2(t)$ will decrease to zero at $t = t_2$ and the second mode is ended at the same time. The duty ratio of the second operation mode can be derived as

$$d_2 = \frac{t_2 - t_1}{T_s} = \frac{-3v_b d_1}{V_{\rm eq} + 3v_b}. \tag{41}$$

At the end of the mode II, the active switch Q_2 is turned off and the values of the other inductor currents at $t = t_2$ can be obtained as

$$i_1(t_2) = -i_3(t_2) = \frac{d_1 T_s}{L} \cdot \frac{V_{\rm eq}(v_b - v_c)}{V_{\rm eq} + 3v_b}. \tag{42}$$

3) Mode III ($t_2 \le t \le t_3$): In the third operation mode, the active switches Q_1 and Q_2 are turned off and the other switch Q_3 is still turned on, as shown in Fig. 7(c). The magnitudes of the inductor currents i_1 and i_3 are continuously decreased and the mathematical expressions are given as

$$L\frac{di_1}{dt} = v_a - V_{\rm eq} - v_{\rm ON} \tag{43}$$

$$L\frac{di_3}{dt} = v_c - v_{\rm ON} \tag{44}$$

where $v_{\rm ON} = (v_a + v_c - V_{\rm eq})/2$. Then, the two inductor currents in the third mode can be derived as

$$i_1(t) = -i_3(t) = \frac{v_a - v_c - V_{\rm eq}}{2L} \cdot (t - t_2) + i_1(t_2). \tag{45}$$

The magnitudes of the two inductor currents will be decreased to zero at the end of the third operation mode simultaneously. Then the duty ratio of the third operation mode $d_3 = (t_3 - t_2)/T_s$ can be derived as

$$d_3 = \frac{-2V_{\rm eq}(v_b - v_c)}{(V_{\rm eq} + 3v_b)(v_a - v_c - V_{\rm eq})} \cdot d_1 \tag{46}$$

4) Mode IV ($t_3 \le t \le t_4$): In the last mode, the three active switches are all turned off and the inductor currents become zero, as illustrated in Fig. 7(d).

The gating signals of the three active switches are shown in Fig. 6(b). The proposed quasi-synchronous rectification technique is to extend the turned on time of respective active switches for reducing the conduction loss. The mathematical expressions of the duty ratio determined by the quasi-synchronous rectification technique in the interval $0 \le \theta_e \le \pi/6$ are summarized as follows:

$$d_{Q_1} = d_1 \tag{47}$$

$$d_{Q_2} = d_1 + d_2 = d_1 \cdot \frac{V_{\rm eq}}{V_{\rm eq} + 3v_b}. \tag{48}$$

$$d_{Q_3} = d_1 + d_2 + d_3 = d_1 \cdot \frac{V_{\rm eq}}{V_{\rm eq} - (v_a - v_c)}. \tag{49}$$

Finally, according to the symmetrical characteristic of the three-phase balance system, the analytic equations of the corresponding duty ratios in one line cycle can be expressed as follows:

$$d_{Q_1} = \begin{cases} d_1, & 0 < \theta_e \le \dfrac{\pi}{2} \text{ and } \dfrac{3\pi}{2} < \theta_e \le 2\pi \\ \dfrac{V_{\rm eq}}{V_{\rm eq} + 3v_a} d_1, & \dfrac{\pi}{2} < \theta_e \le \dfrac{2\pi}{3} \text{ and } \dfrac{4\pi}{3} < \theta_e \le \dfrac{3\pi}{2} \\ \dfrac{V_{\rm eq}}{V_{\rm eq} - (v_b - v_a)} d_1, & \dfrac{2\pi}{3} < \theta_e \le \pi \\ \dfrac{V_{\rm eq}}{V_{\rm eq} - (v_c - v_a)} d_1, & \pi < \theta_e \le \dfrac{4\pi}{3} \end{cases} \tag{50}$$

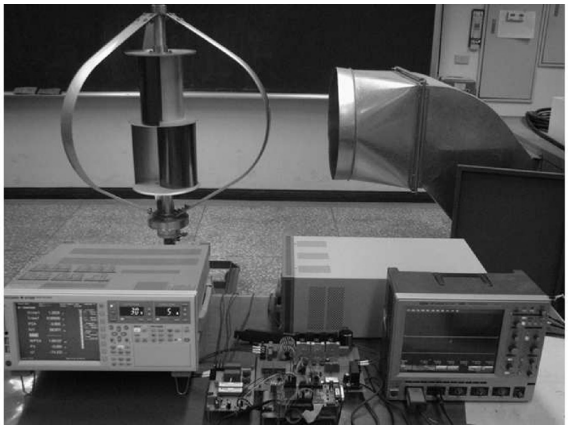

Fig. 8. Test facility of the implemented prototype system.

$$d_{Q2} = \begin{cases} \dfrac{V_{\rm eq}}{V_{\rm eq}+3v_b}d_1, & 0<\theta_e\le\dfrac{\pi}{6} \text{ and } \dfrac{7\pi}{6}<\theta_e\le\dfrac{4\pi}{3} \\ d_1, & \dfrac{\pi}{6}<\theta_e\le\dfrac{7\pi}{6} \\ \dfrac{V_{\rm eq}}{V_{\rm eq}-(v_c-v_b)}d_1, & \dfrac{4\pi}{3}<\theta_e\le\dfrac{5\pi}{3} \\ \dfrac{V_{\rm eq}}{V_{\rm eq}-(v_a-v_b)}d_1, & \dfrac{5\pi}{3}<\theta_e\le 2\pi \end{cases} \tag{51}$$

$$d_{Q3} = \begin{cases} \dfrac{V_{\rm eq}}{V_{\rm eq}-(v_a-v_c)}d_1, & 0<\theta_e\le\dfrac{\pi}{3} \\ \dfrac{V_{\rm eq}}{V_{\rm eq}-(v_b-v_c)}d_1, & \dfrac{\pi}{3}<\theta_e\le\dfrac{2\pi}{3} \\ \dfrac{V_{\rm eq}}{V_{\rm eq}+3v_c}d_1, & \dfrac{2\pi}{3}<\theta_e\le\dfrac{5\pi}{6} \text{ and } \dfrac{11\pi}{6}<\theta_e\le 2\pi \\ d_1, & \dfrac{5\pi}{6}<\theta_e\le\dfrac{11\pi}{6}. \end{cases} \tag{52}$$

Consequently, the extended turn-ON time for the respective switches can be determined straightforward from the derived analytic equations of the duty ratios.

V. Experimental Results

To verify the validity and performance of the proposed MPPT controller, a prototype is constructed, as shown in Fig. 8, and some experiments are carried out. The parameters of the prototype are given in Table I for reference. The vertical-axis wind turbine DS-200 is manufactured by HiEnergy Technology Company Ltd. The MOSFETs, IXFH150N15P, and Schottky rectifiers, DSSK20-015 A, are used for the active switches and diodes of the ac-to-dc converter. The proposed MPPT controller shown in Fig. 4 and the analytic closed form duty ratio of the quasi-synchronous rectification ac-to-dc converter as described from (50) to (52) are all implemented with a DSP, TMS320F2812. A precision power analyzer WT3000 manufactured by Yokogawa Electric Corporation is used to measure the experimental data. The dc-link voltage of the prototype converter is set to 100 V and the switching frequency is 25 kHz.

TABLE I
System Parameters of the Proposed Microscale WPGS

Radius of the wind turbine r	0.5 m
Total inertia J	0.4 $k_g \cdot m^2$
Viscous damping coefficient B	0.008
Rated Power	200 w
Rated wind speed	12.5 m/s
Stator inductance L_s	70 uH
Boost inductor L	22 uH
Filter capacitor C_f	4.7 uF
Maximum power coefficient $C_{p,max}$	0.2812
Optimal TSR δ_{opt}	3.53

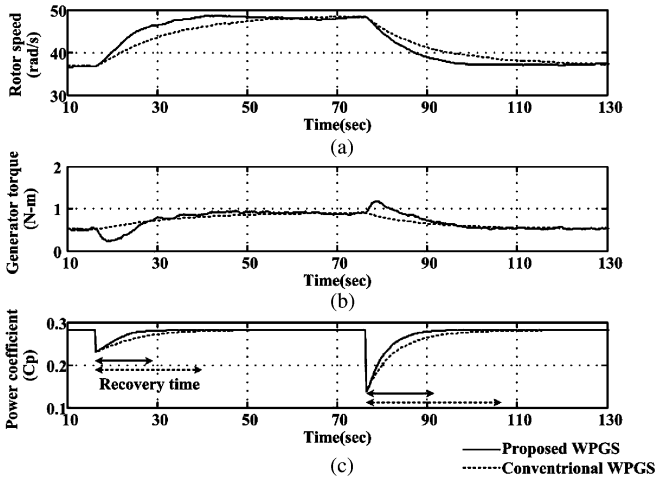

Fig. 9. Experimental results under step changing wind speed. (a) Rotor speed. (b) Generator torque. (c) Power coefficient.

First, to demonstrate the function of the proposed MPPT controller, the system is tested under changing wind speed situation and the corresponding experimental results are shown in Fig. 9. It is seen from Fig. 9(b) that as the wind speed steps up to a higher speed, the generator torque in the proposed system is instantly controlled to be smaller than that of the conventional system for achieving faster converging to the optimal operating point. On the contrary, as the wind speed steps down to a lower speed, the torque command will be instantly controlled to a larger magnitude for decelerating the wind turbine more rapidly to the optimal operating point. Fig. 9(c) shows the corresponding power coefficients, which are calculated from the measured data with the approximate polynomial of the C_p function. It can be seen from Fig. 9(c) that as a result of the improved dynamic response, the regulation of the power coefficient of the wind turbine is greatly enhanced. Next, to evaluate the performance of energy extraction, the variation of the wind speed is given as follows [19], [23]:

$$v_w(t) = 6.25\left[1 + 0.09\sin\left(\frac{2\pi}{20}t\right) + 0.15\sin\left(\frac{2\pi}{50}t\right)\right]. \tag{53}$$

According to (29), the bandwidth of the dynamic response of the conventional system is about 0.03 Hz. Therefore, the energy

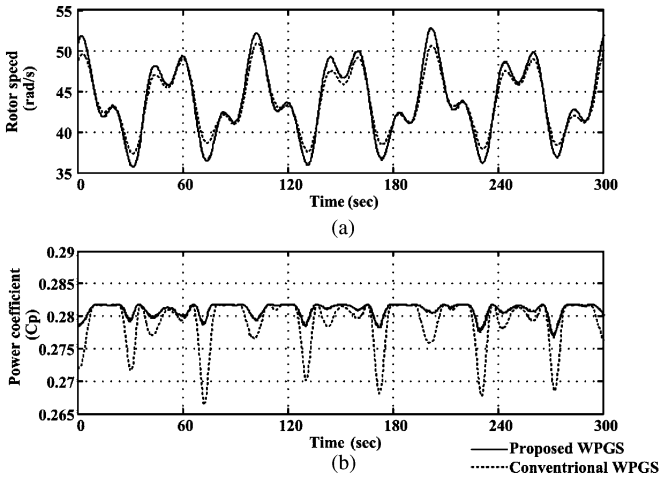

Fig. 10. Experimental results under continuously varying wind speed. (a) Rotor speed. (b) Power coefficient.

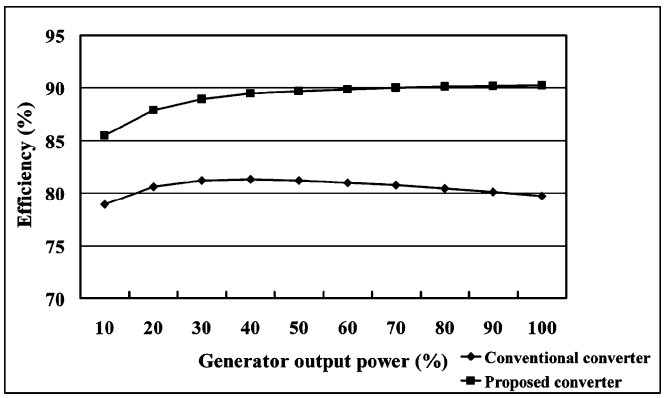

Fig. 11. Experimentally measured efficiencies of the proposed and conventional converters.

of the higher frequency wind speed variation term in (53) will not be fully extracted. However, the bandwidth of the proposed system can be set to 0.1 Hz according to (32). The rotor speed and the calculated power coefficient are shown in Fig. 10(a) and (b). It can be seen from Fig. 10(b) that due to the improved dynamic response the regulation of the power coefficient of the proposed WPGS is greatly improved. Hence, the proposed system can effectively extract more wind energy from the higher frequency wind speed variation. Furthermore, both the proposed single-stage quasi-synchronous rectification ac-to-dc converter and the conventional two-stage converter with a diode bridge rectifier are constructed and the efficiencies of the proposed single-stage rectifier and the conventional two-stage converter are compared with respect to the generator output power, as shown in Fig. 11. The generator output power is controlled to track the maximum power curve as expressed in (4). In the proposed rectifier, due to the reduction of the number of the diodes, the conduction losses of the diodes are reduced first. Moreover, because the diodes in the proposed rectifier are all turned off with zero current switching, the well-known reverse recovery losses are also eliminated. Therefore, the efficiency of the proposed rectifier may be greatly improved to about 90.2% at the rated power, as shown in Fig. 11.

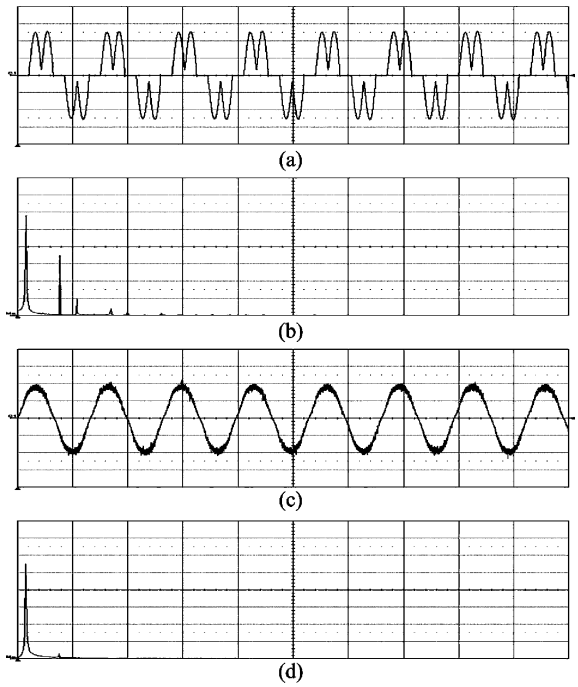

Fig. 12. Experimental results (10 ms/division). (a) Generator current of the conventional system (2 A/division). (b) FFT of the generator current (500 Hz/division). (c) Generator current of the proposed system (2 A/division). (d) FFT of the generator current in (c) (500 Hz/division).

A main drawback of the conventional two-stage converter is the significant THD of the generator current, as shown in Fig. 12(a) and (b). As a comparison, the generator current of the proposed system is shown in Fig. 12(c) and the corresponding FFT of the generator current is shown in Fig. 12(d). The THD of the generator current is obviously greatly reduced in the proposed system. After an integration period of 500 s, under the wind speed variation, as given in (53), the extracted wind energy of the proposed system and the conventional system are 4.570 and 4.467 Wh, respectively. The total output energy of the proposed system and that of the conventional system are 4.040 and 3.575 Wh, respectively. It is found that the output energy from the proposed WPGS can be increased by 13% approximately as compared with the conventional system. To further evaluate the performance of the proposed controller under significative wind gust, a simulation case is carried out with the wind velocity expressed as follows [23]:

$$v_w(t) = V_w + v_g(t) \tag{54}$$

where V_w is the mean value of the wind velocity and $v_g(t)$ is the model of the wind gust that can be defined by the following equation:

$$v_g(t) = \frac{2v_{g\max}}{1 + e^{-4(\sin(\omega_g t)-1)}} \tag{55}$$

where $v_{g\max}$ is the gust amplitude and $\omega_g = 2\pi/T_g$ is the gust frequency. In this simulation, the mean value of the wind velocity is considered as 6 m/s, the gust amplitude is taken as 25% and the period, T_g, is chosen to be 10 s [19], [23]. To make the simulation results more close to the implementation, the relative

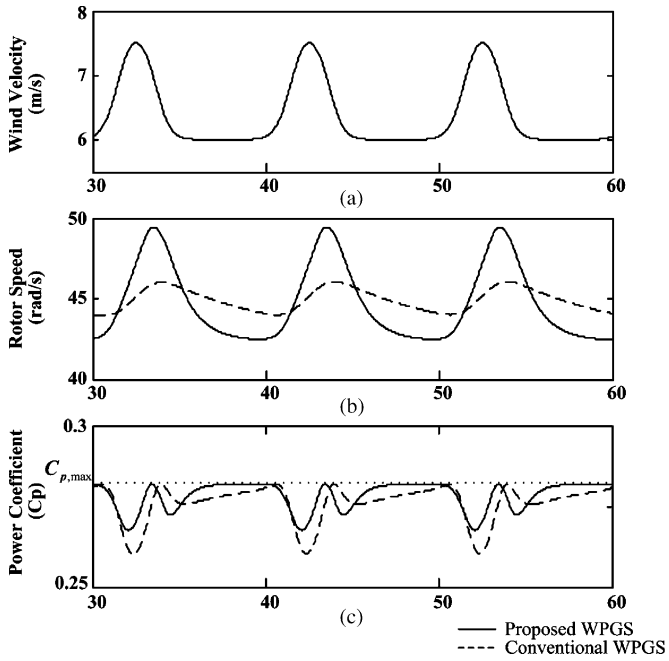

Fig. 13. Simulation waveforms with gusty wind velocity: (a) wind velocity, (b) rotor speed, and (c) power coefficient.

parameters are all chosen to follow closely the practical system parameters, as shown in Table I. Fig. 13 shows the simulated dynamic response of the proposed and the conventional systems to the gusty wind velocity as mentioned above. It is seen that the dynamic response of the rotor speed of the wind turbine is greatly improved and the resulting power coefficient of the proposed WPGS also can be maintained more closely to optimal value more rapidly. However, due to lack of the desired facility, the corresponding experiment cannot be carried out currently in the authors' laboratory. From the previous experimental and simulation results one can see that both the dynamic performance of MPPT controller and the QSR ac-to-dc converter indeed can contribute to the efficiency improvement significantly in the proposed WPGS. Compared with the two-stage converter, the proposed converter consists of only three smaller filter capacitors, three smaller boost inductors, three diodes, and three MOSFETs. Although the cost of the proposed rectifier may be a little more than the traditional two-stage converter. However, from the results in the proposed paper, it can be seen that not only the generator current THD can be reduced greatly but also the efficiency of the converter can be enhanced to about 90.2% under rated power condition. The mechanical vibration due to the torque ripple will also be reduced so that less environment noise is made. Moreover, because of the improving of the efficiency, the payback period, the time needed to recoup the system cost, may also be shorten.

VI. Conclusion

In this paper, a novel MPPT controller with an adaptive compensation control has been first proposed for a microscale WPGS. Due to the adaptive compensation control effort, the dynamic response has been improved and more wind energy can be extracted during wind velocity variations. To reduce cost and enhance reliability, there is no any mechanical sensor necessary in this proposed WPGS. For achieving higher efficiency and lower THD, a single-stage ac-to-dc converter has then been proposed to replace the traditional two-stage converter and incorporate the MPPT control. To further improve the efficiency of the converter, a QSR algorithm is proposed to control the active switches for reducing the conduction loss of the body diodes. The analytic equations of duty ratios of the corresponding active switches are also derived for easy implementation. Furthermore, a prototype system is constructed and the proposed MPPT controller and QSR algorithm are both implemented using a DSP, namely, TMS320 F2812. Some experimental results are given to verify the validity of the proposed microscale WPGS. It is found that the total output energy can be increased significantly.

References

[1] AWEA. (2007, Jul.). AWEA small wind turbine global market study 2007, in *The American Wind Energy Association Small Wind Systems* [Online]. Available: http://www.awea.org/smallwind/

[2] A. M. Knight and G. E. Peters, "Simple wind energy controller for an expanded operation range," *IEEE Trans. Energy Convers.*, vol. 20, no. 2, pp. 459–466, Jun. 2005.

[3] S. Morimoto, H. Nakayama, M. Sanada, and Y. Takeda, "Sensorless output maximization control for variable-speed wind generation system using IPMSG," *IEEE Trans. Ind. Appl.*, vol. 41, no. 1, pp. 60–67, Jan./Feb. 2005.

[4] K. Tan and S. Islam, "Optimum control strategies in energy conversion of PMSG wind turbine system without mechanical sensors," *IEEE Trans. Energy Convers.*, vol. 19, no. 2, pp. 392–399, Jun. 2004.

[5] F. Valenciaga and P. F. Puleston, "Supervisor control for a stand-alone hybrid generation system using wind and photovoltaic energy," *IEEE Trans. Energy Convers.*, vol. 20, no. 2, pp. 398–405, Jun. 2005.

[6] E. Koutroulis and K. Kalaitzakis, "Design of a maximum power tracking system for wind-energy-conversion applications," *IEEE Trans. Ind. Electron.*, vol. 53, no. 2, pp. 486–494, Apr. 2006.

[7] R. Datta and V. T Ranganathan, "A method of tracking the peak power points for a variable speed wind energy conversion system," *IEEE Trans. Energy Convers.*, vol. 18, no. 1, pp. 163–168, Mar. 2003.

[8] P. Vas, *Vector Control of AC Machines*. New York: Oxford Univ. Press, 1990.

[9] T. Emura, L. Wang, M. Yamanaka, and H. Nakamura, "A high-precision positioning servo controller based on phase/frequency detecting technique of two-phase-type PLL," *IEEE Trans. Ind. Electron.*, vol. 47, no. 6, pp. 1298–1306, Dec. 2000.

[10] G. F. Franklin, J. D. Powell, and A. Emami-Naeini, *Feedback Control of Dynamic Systems*. Englewood Cliffs, NJ: Prentice-Hall, 2002.

[11] A. R. Prasad, P. D. Ziogas, and S. Manias, "An active power factor correction technique for three-phase diode rectifier," *IEEE Trans. Power Electron.*, vol. 6, no. 1, pp. 83–92, Jan. 1991.

[12] A. E. Feijoo, J. Cidras, and J. L. G. Dornelas, "Wind speed simulation in wind farms for steady-state security assessment of electrical power systems," *IEEE Trans. Energy Convers.*, vol. 14, no. 4, pp. 1582–1588, Dec. 1999.

[13] G. Hua and Y. Geng, "A novel control strategy of MPPT taking dynamics of wind turbine into account," in *Proc. IEEE PESC 2006*, Jeju, Korea, Jun. 18–22, pp. 1–6.

[14] M. Chinchilla, S. Arnaltes, and J. C. Burgos, "Control of permanent-magnet generators applied to variable-speed wind-energy systems connected to the grid," *IEEE Trans. Energy Convers.*, vol. 21, no. 1, pp. 130–135, Mar. 2006.

[15] J. A. Baroudi, V. Dinavahi, and A. M. Knight, "A review of power converter topologies for wind generators," in *Proc. IEEE Int. Conf. Electr. Mach. Drives*, May 15–18, 2005, pp. 458–465.

[16] F. S. Dos Reis, S. Islam, K. Tan, J. V. Alé, F. D. Adegas, and R. Tonkoski Jr., "Harmonic mitigation in wind turbine energy conversion systems," in *Proc. IEEE PESC 2006*, Jeju, Korea, Jun. 18–22, pp. 2748–2754.

[17] F. J. Lin and Y. S. Lin, "A robust PM synchronous motor drive with adaptive uncertainty observer," *IEEE Trans. Energy Convers.*, vol. 14, no. 4, pp. 989–995, Dec. 1999.
[18] AWEA. (2002, Jun.). The U.S. small wind turbine industry roadmap: A 20-year industry plan for small wind turbine technology, in *The American Wind Energy Association Small Wind Systems* [Online]. Available: http://www.awea.org/smallwind/
[19] M. Karrari, W. Rosehart, and O. P. Malik, "Comprehensive control strategy for a variable speed cage machine wind generation unit," *IEEE Trans. Energy Convers.*, vol. 20, no. 2, pp. 415–423, Jun. 2005.
[20] A. Mirecki, X. Roboam, and F. Richardeau, "Architecture complexity and energy efficiency of small wind turbines," *IEEE Trans. Ind. Electron.*, vol. 54, no. 1, pp. 660–670, Feb. 2007.
[21] B. Beltran, T. Ahmed-Ali, and M. E. H. Benbouzid, "Sliding mode power control of variable-speed wind energy conversion systems," *IEEE Trans. Energy Convers.*, vol. 23, no. 2, pp. 551–558, Jun. 2008.
[22] S. K. Chung, J. H. Lee, J. S. Ko, and M. J. Youn, "Robust speed control of brushless direct-drive motor using integral variable structure control," in *IEE Proc. Electr. Power Appl.*, vol. 142, no. 6, pp. 361–370, Nov. 1995.
[23] Z. Lubosny, *Wind Turbine Operation in Electric Power Systems: Advance Modeling*. Berlin, Germany: Springer-Verlag, 2003.

Ching-Tsai Pan (M'88) was born in Taipei, Taiwan, in 1948. He received the B.S. degree from National Cheng Kung University, Tainan, Taiwan, in 1970, and the M.S. and Ph.D. degrees from Texas Tech University, Lubbock, in 1974 and 1976, respectively, all in electrical engineering.

Since 1977, he has been with the Department of Electrical Engineering, National Tsing Hua University, Hsinchu, Taiwan, where he is currently a Tsing Hua Chair Professor and the Director of the Center for Teaching and Learning Development. He was the Director of the University Computer Center and the Ministry of Education, from 1986 to 1989 and from 1989 to 1992, respectively. He was also the Chairman of the Department of Electrical Engineering and the Director of the University Library, from 1994 to 1997 and from 2000 to 2002, respectively. In addition, from 2003 to 2008, he was also the Founder and the Director of the Center for Advanced Power Technologies. His current research interests include power electronics, ac motor drives, control systems, power systems, and numerical analysis. He holds more than 40 patents. He has authored or coauthored more than 310 technical papers published in various journals and conference proceedings.

Dr. Pan is the recipient of the Award for Excellence in Teaching from the Ministry of Education and of the Outstanding Research Award from the National Science Council. He is a member of the Chinese Institute of Engineers, the Chinese Institute of Electrical Engineering, the Chinese Institute of Automatic Control Engineering, the Chinese Institute of Computer Society, the Taiwan Association of System Science and Engineering, the Taiwan Power Electronics Association, the Taiwan Wind Energy Association, the Phi Tau Phi, the Eta Kappa Nu, and the Phi Kappa Phi. He received the Merit National Science Council Research Fellow Award of R.O.C. in 2008. He was also the Chairman of the IEEE Industrial Electronics Society, the IEEE Power Engineering Society, and the IEEE Power Electronics Society, Taipei Sections.

Yu-Ling Juan (S'08) was born in Kaohsiung, Taiwan, in 1979. He received the B.S. degree in electrical engineering from National Cheng Kung University, Tainan, Taiwan, in 2001 and the M.S. degree in electrical engineering in 2003 from National Tsing Hua University, Hsinchu, Tawan, where he is currently working toward the Ph.D. degree in electrical engineering.

His current research interests include power electronics, renewable energy systems, and ac motor drives.